

# Semiconductor saturable absorber Q-switching of a holmium micro-laser

RUIJUN LAN,<sup>1,2</sup> XAVIER MATEOS,<sup>1,3,6,\*</sup> YICHENG WANG,<sup>1</sup> JOSEP MARIA SERRES,<sup>3</sup> PAVEL LOIKO,<sup>4</sup> JIANG LI,<sup>5</sup> YUBAI PAN,<sup>5</sup> UWE GRIEBNER,<sup>1</sup> AND VALENTIN PETROV<sup>1</sup>

<sup>1</sup>Max Born Institute for Nonlinear Optics and Short Pulse Spectroscopy, Max-Born-Str. 2a, D-12489 Berlin, Germany

<sup>2</sup>School of Opto-Electronic Information Science and Technology, Yantai University, 264005 Yantai, China

<sup>3</sup>Física i Cristal·lografia de Materials i Nanomaterials (FiCMA-FiCNA), Universitat Rovira i Virgili (URV), Campus Sescelades, c/ Marcel·lí Domingo, s/n., E-43007 Tarragona, Spain

<sup>4</sup>ITMO University, 49 Kronverkskiy pr., 197101 St. Petersburg, Russia

<sup>5</sup>Key Laboratory of Transparent and Opto-Functional Inorganic Materials, CAS Shanghai Institute of Ceramics, Chinese Academy of Sciences, 1295 Dingxi Road, 200050 Shanghai, China

<sup>6</sup>xavier.mateos@urv.cat

\*mateos@mbi-berlin.de

**Abstract:** We report on a Holmium micro-laser passively Q-switched by a semiconductor saturable absorber (SSA), for the first time to the best of our knowledge. It is based on a 1 at.% Ho:YAG ceramic with good energy storage capability and several commercial transmission-type SSAs with 0.24% modulation depth. Under in-band pumping by a Tm fiber laser at 1910 nm, the Ho micro-laser generated 450 mW at 2089 nm with 37% slope efficiency. Stable 89 ns, 3.2  $\mu$ J pulses are achieved at a repetition rate of 141 kHz. Further shortening of the laser pulses is feasible with the increase of the modulation depth of the SSA while power scaling may lead to Q-switching at MHz-range repetition rates.

© 2017 Optical Society of America

**OCIS codes:** (140.3380) Laser materials; (140.3480) Lasers, diode-pumped; (140.3540) Lasers, Q-switched.

## References and links

1. J. Dong, K. Ueda, A. Shirakawa, H. Yagi, T. Yanagitani, and A. A. Kaminskii, "Composite Yb:YAG/Cr<sup>4+</sup>:YAG ceramics picosecond microchip lasers," *Opt. Express* **15**(22), 14516–14523 (2007).
2. A. Ikesue, T. Kinoshita, K. Kamata, and K. Yoshida, "Fabrication and optical properties of high-performance polycrystalline Nd:YAG ceramics for solid-state lasers," *J. Am. Ceram. Soc.* **78**(4), 1033–1040 (1995).
3. W. L. Gao, J. Ma, G. Q. Xie, J. Zhang, D. W. Luo, H. Yang, D. Y. Tang, J. Ma, P. Yuan, and L. J. Qian, "Highly efficient 2  $\mu$ m Tm:YAG ceramic laser," *Opt. Lett.* **37**(6), 1076–1078 (2012).
4. T. Zhao, H. Chen, D. Y. Shen, Y. Wang, X. F. Yang, J. Zhang, H. Yang, and D. Y. Tang, "Effects of Ho<sup>3+</sup>-doping concentration on the performances of resonantly pumped Ho:YAG ceramic lasers," *Opt. Mater.* **35**(4), 712–714 (2013).
5. H. Yang, J. Zhang, X. P. Qin, D. W. Luo, J. Ma, D. Y. Tang, H. Chen, D. Y. Shen, and Q. T. Zhang, "Polycrystalline Ho:YAG transparent ceramics for eye-safe solid state laser applications," *J. Am. Ceram. Soc.* **95**(1), 52–55 (2012).
6. H. Chen, D. Shen, J. Zhang, H. Yang, D. Tang, T. Zhao, and X. Yang, "In-band pumped highly efficient Ho:YAG ceramic laser with 21 W output power at 2097 nm," *Opt. Lett.* **36**(9), 1575–1577 (2011).
7. P. Loiko, J. M. Serres, X. Mateos, K. Yumashev, N. Kuleshov, V. Petrov, U. Griebner, M. Aguiló, and F. Díaz, "In-band-pumped Ho:KLu(WO<sub>4</sub>)<sub>2</sub> microchip laser with 84% slope efficiency," *Opt. Lett.* **40**(3), 344–347 (2015).
8. J. J. Zayhowski and C. Dill, "Diode-pumped passively Q-switched picosecond microchip lasers," *Opt. Lett.* **19**(18), 1427–1429 (1994).
9. B. Yao, J. Yuan, J. Li, T. Dai, X. Duan, Y. Shen, Z. Cui, and Y. Pan, "High-power Cr<sup>2+</sup>:ZnS saturable absorber passively Q-switched Ho:YAG ceramic laser and its application to pumping of a mid-IR OPO," *Opt. Lett.* **40**(3), 348–351 (2015).
10. P. Loiko, J. M. Serres, X. Mateos, K. Yumashev, A. Yasukevich, V. Petrov, U. Griebner, M. Aguiló, and F. Díaz, "Subnanosecond Tm:KLuW microchip laser Q-switched by a Cr:ZnS saturable absorber," *Opt. Lett.* **40**(22), 5220–5223 (2015).
11. U. Keller, K. J. Weingarten, F. X. Kartner, D. Kopf, B. Braun, I. D. Jung, R. Fluck, C. Honninger, N. Matuschek, and J. Aus der Au, "Semiconductor saturable absorber mirrors (SESAM's) for femtosecond to nanosecond pulse generation in solid-state lasers," *IEEE J. Sel. Top. Quantum Electron.* **2**(3), 435–453 (1996).

12. B. Braun, F. X. Kärtner, G. Zhang, M. Moser, and U. Keller, "56-ps passively Q-switched diode-pumped microchip laser," *Opt. Lett.* **22**(6), 381–383 (1997).
13. G. J. Spühler, R. Paschotta, M. P. Kullberg, M. Graf, M. Moser, E. Mix, G. Huber, C. Harder, and U. Keller, "A passively Q-switched Yb:YAG microchip laser," *Appl. Phys. B* **72**(3), 285–287 (2001).
14. F. Di Teodoro and C. D. Brooks, "Multistage Yb-doped fiber amplifier generating megawatt peak-power, subnanosecond pulses," *Opt. Lett.* **30**(24), 3299–3301 (2005).
15. Y. Wang, G. Xie, X. Xu, J. Di, Z. Qin, S. Suomalainen, M. Guina, A. Härkönen, A. Agnesi, U. Griebner, X. Mateos, P. Loiko, and V. Petrov, "SESAM mode-locked Tm:CALGO laser at 2  $\mu\text{m}$ ," *Opt. Mater. Express* **6**(1), 131–136 (2016).
16. G. Q. Xie, J. Ma, P. Lv, W. L. Gao, P. Yuan, L. J. Qian, H. H. Yu, H. J. Zhang, J. Y. Wang, and D. Y. Tang, "Graphene saturable absorber for Q-switching and mode locking at 2  $\mu\text{m}$  wavelength," *Opt. Mater. Express* **2**(6), 878–883 (2012).
17. W. B. Cho, J. H. Yim, S. Y. Choi, S. Lee, A. Schmidt, G. Steinmeyer, U. Griebner, V. Petrov, D.-I. Yeom, K. Kim, and F. Rotermund, "Boosting the nonlinear optical response of carbon nanotube saturable absorbers for broadband mode-locking of bulk lasers," *Adv. Funct. Mater.* **20**(12), 1937–1943 (2010).
18. M. Gaponenko, N. Kuleshov, and T. Südmeyer, "Passively Q-switched thulium microchip laser," *IEEE Photonics Technol. Lett.* **28**(2), 147–150 (2016).
19. J. M. Serres, P. Loiko, X. Mateos, K. Yumashev, U. Griebner, V. Petrov, M. Aguiló, and F. Díaz, "Tm:KLu(WO<sub>4</sub>)<sub>2</sub> microchip laser Q-switched by a graphene-based saturable absorber," *Opt. Express* **23**(11), 14108–14113 (2015).
20. P. Loiko, X. Mateos, S. Y. Choi, F. Rotermund, J. M. Serres, M. Aguiló, F. Díaz, K. Yumashev, U. Griebner, and V. Petrov, "Vibronic thulium laser at 2131 nm Q-switched by single-walled carbon nanotubes," *J. Opt. Soc. Am. B* **33**(11), D19–D27 (2016).
21. J. Li, J. Zhou, Y. B. Pan, W. B. Liu, W. X. Zhang, J. K. Guo, H. Chen, D. Y. Shen, X. F. Yang, and T. Zhao, "Solid-state reactive sintering and optical characteristics of transparent Er:YAG laser ceramics," *J. Am. Ceram. Soc.* **95**(3), 1029–1032 (2012).
22. J. Li, J. Liu, B. L. Liu, W. B. Liu, Y. P. Zeng, X. W. Ba, T. F. Xie, B. X. Jiang, Q. Liu, Y. B. Pan, X. Q. Feng, and J. K. Guo, "Influence of heat treatment of powder mixture on the microstructure and optical transmission of Nd:YAG transparent ceramics," *J. Eur. Ceram. Soc.* **34**(10), 2497–2507 (2014).
23. B. M. Walsh, G. W. Grew, and N. P. Barnes, "Energy levels and intensity parameters of Ho<sup>3+</sup> ions in Y<sub>3</sub>Al<sub>5</sub>O<sub>12</sub> and Lu<sub>3</sub>Al<sub>5</sub>O<sub>12</sub>," *J. Phys. Chem. Solids* **67**(7), 1567–1582 (2006).
24. R. Lan, P. Loiko, X. Mateos, Y. Wang, J. Li, Y. Pan, S. Y. Choi, M. H. Kim, F. Rotermund, A. Yasukevich, K. Yumashev, U. Griebner, and V. Petrov, "Passive Q-switching of microchip lasers based on Ho:YAG ceramics," *Appl. Opt.* **55**(18), 4877–4887 (2016).
25. T. Zhao, Y. Wang, H. Chen, and D. Y. Shen, "Graphene passively Q-switched Ho:YAG ceramic laser," *Appl. Phys. B* **116**(4), 947–950 (2014).
26. P. Loiko, J. M. Serres, X. Mateos, K. Yumashev, A. Malyarevich, A. Onushchenko, V. Petrov, U. Griebner, M. Aguiló, and F. Díaz, "Ho:KLu(WO<sub>4</sub>)<sub>2</sub> microchip laser Q-switched by a PbS quantum-dot-doped glass," *IEEE Photonics Technol. Lett.* **27**(17), 1795–1798 (2015).

## 1. Introduction

Nowadays, the transparent ceramics technology becomes a competitor of the single-crystal growth because ceramics possess high optical quality, are cost-effective and size-scalable. In particular, the fabrication of ceramics based on cubic Y<sub>3</sub>Al<sub>5</sub>O<sub>12</sub> (YAG) doped with various rare-earth ions, e.g. Nd<sup>3+</sup> or Yb<sup>3+</sup>, is well-established for efficient lasers at ~1  $\mu\text{m}$  [1,2]. At ~2  $\mu\text{m}$ , the research focused on doping of YAG ceramics with Tm<sup>3+</sup> [3] and, recently, also with Ho<sup>3+</sup> ions [4,5]. The Ho<sup>3+</sup> ion is known for its <sup>5</sup>I<sub>7</sub> → <sup>5</sup>I<sub>8</sub> eye-safe emission occurring at wavelengths slightly above 2  $\mu\text{m}$  with high relevance for medical applications. Efficient and power-scalable laser operation with Ho:YAG ceramics has been recently reported using in-band pumped configurations (Tm laser pumping into the upper laser level (<sup>5</sup>I<sub>7</sub>) of Ho<sup>3+</sup>) [4–6]. This scheme is known for reaching high efficiency of the Ho lasers [7].

Passive Q-switching (PQS) of a solid-state laser by the introduction of an appropriate saturable absorber (SA) is a relatively simple approach to generate nanosecond pulses and to design such all-solid-state and compact coherent sources. The latter feature can be even more efficiently exploited in microchip lasers with both the laser element and the SA placed in a short plano-plano laser cavity providing a very short cavity round trip time [8]. Well recognized "slow" SAs for ~1  $\mu\text{m}$  and ~2  $\mu\text{m}$  lasers are dielectric crystals doped with transition-metal ions, e.g. Cr<sup>4+</sup>:YAG [1] and Cr<sup>2+</sup>:ZnS [9,10], respectively. Such SAs enable the generation of high pulse energies (from hundreds of  $\mu\text{J}$  up to few mJ) at low repetition rates. As for "fast" SAs at ~1  $\mu\text{m}$ , the most widespread and commercialized are the Semiconductor Saturable Absorbers (SSAs) providing low saturation intensity, fast (ps-long) recovery time of the initial absorption, low non-saturable losses and acceptable laser-induced

damage threshold (LIDT) [11]. SSAs employed in microchip lasers at  $\sim 1 \mu\text{m}$  enabled the generation of sub-ns pulses at high repetition frequencies (hundreds of kHz – few MHz) while the pulse energy was about few  $\mu\text{J}$  [12,13]. In addition, such microchip lasers are very attractive for seeding high-pulse-energy amplifiers [14].

The application of SSAs at  $\sim 2 \mu\text{m}$  is still not well established [15]. This is partially related to the more complex technology of their manufacturing for operation in this spectral range, lower LIDT and higher non-saturable losses. Thus, an active search of alternative materials is still ongoing. Most promising at  $\sim 2 \mu\text{m}$  seem “fast” SAs based on carbon nanostructures such as graphene or single-walled carbon nanotubes (SWCNTs) [16,17]. A reflection-type SSA (SESAM) has been recently employed in a passively Q-switched Tm microchip laser generating  $0.11 \mu\text{J} / 2.4 \text{ ns}$  pulses at 1905 nm with a repetition rate of 1.2 MHz [18]. The application of graphene- and SWCNT-SAs in Tm microchip lasers led to higher pulse energies (few  $\mu\text{J}$ ) but longer pulse durations [19,20], e.g., for SWCNT-SA, 25-40 ns pulses were generated [20].

In the present work, we aimed to realize the first Ho microchip-type laser Q-switched by a commercial transmission-type SSA and to exploit the potential of such SAs for the generation of ns pulses at  $\sim 2.1 \mu\text{m}$ .

## 2. Experimental

### 2.1 Ho:YAG laser ceramics

The 1 at.% Ho:YAG transparent ceramics ( $N_{\text{Ho}} = 1.4 \times 10^{20} \text{ cm}^{-3}$ ) was prepared by a solid-state reaction and vacuum sintering method using commercial  $\text{Y}_2\text{O}_3$ ,  $\alpha\text{-Al}_2\text{O}_3$  and  $\text{Ho}_2\text{O}_3$  as starting powders, see [21,22] for details. The 1 at.% Ho doping was selected to prevent the deterioration of the laser efficiency due to upconversion losses [4]. The laser element was 4-mm thick, with both faces ( $3 \times 3 \text{ mm}^2$ ) polished to laser quality and uncoated. This thickness of the laser element was selected in order to benefit from the short geometrical cavity length and, hence, short cavity roundtrip time in a passively Q-switched laser. At first, we determined the absorption,  $\sigma_{\text{abs}}$ , and stimulated-emission,  $\sigma_{\text{SE}}$ , cross-sections of  $\text{Ho}^{3+}$  in the YAG ceramics corresponding to the  ${}^5\text{I}_8 \leftrightarrow {}^5\text{I}_7$  transition, as shown in Fig. 1(a). The  $\sigma_{\text{abs}}$  was determined as  $\alpha/N_{\text{Ho}}$  where  $\alpha$  is the measured absorption coefficient and  $\sigma_{\text{SE}}$  was determined with the reciprocity method using the reported Stark splitting for the Ho:YAG single-crystal in [23]. The maximum  $\sigma_{\text{abs}}$  is  $0.98 \times 10^{-20} \text{ cm}^2$  at 1906.5 nm (full width at half maximum, FWHM, of this peak is 5.6 nm) and the maximum  $\sigma_{\text{SE}}$  is  $1.44 \times 10^{-20} \text{ cm}^2$  at 2090.1 nm. The radiative lifetime of  $\text{Ho}^{3+}$  in the upper laser level,  $\tau_{\text{rad}}({}^5\text{I}_7) = 7.7 \text{ ms}$  was estimated from the Judd-Ofelt modeling.

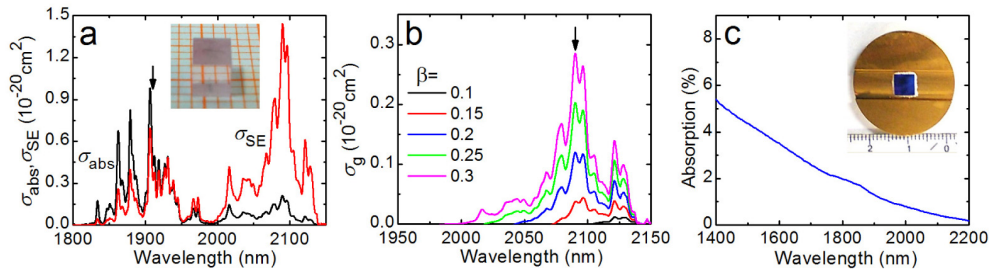


Fig. 1. Spectroscopy of 1 at.% Ho:YAG ceramics: (a) absorption,  $\sigma_{\text{abs}}$ , and stimulated-emission,  $\sigma_{\text{SE}}$ , cross-section spectra and (b) gain,  $\sigma_g = \beta\sigma_{\text{SE}} - (1-\beta)\sigma_{\text{abs}}$ , cross-section spectra,  $\beta$  is the inversion ratio, arrows denote pump (a) and laser (b) wavelengths for the Ho:YAG ceramic laser; inset of (a) – photograph of the studied sample; (c) Low intensity absorption spectrum of the transmission-type semiconductor saturable absorber (SSA), inset: image of the studied SSA mounted on a Cu-holder.

The  $\text{Ho}^{3+}$  ion represents a quasi-three-level laser scheme. Thus, we have also determined the gain cross-sections,  $\sigma_g = \beta\sigma_{\text{SE}} - (1-\beta)\sigma_{\text{abs}}$ , where  $\beta = N({}^5\text{I}_7)/N_{\text{Ho}}$  is the inversion ratio, Fig.

1(b). For low  $\beta < 0.15$ , local maxima at 2121 and 2128 nm are observed in the gain spectra. For higher inversion levels, laser operation is expected at 2096 nm ( $\beta < 0.2$ ) and at 2090 nm ( $\beta > 0.2$ ). The studied Ho:YAG ceramic has a slight rose coloration due to the Ho<sup>3+</sup> dopant, with high optical quality. The loss coefficient estimated from modeling of the continuous-wave (CW) laser performance [24] was  $\delta_{\text{loss}} = 0.0056 \text{ cm}^{-1}$  at  $\sim 2090 \text{ nm}$ .

## 2.2 Laser set-up

The laser performance of the Ho:YAG ceramic was studied in a plano-plano (microchip-type) laser cavity. The laser cavity consisted of a flat pump mirror (PM) coated for high reflection (HR) at 2.0-2.15  $\mu\text{m}$  and high transmission (HT) around 1.91  $\mu\text{m}$ , and a flat output coupler (OC) with a transmission of 10% at 1.9-2.15  $\mu\text{m}$ . The laser element was wrapped with Indium foil and mounted in a Cu-holder providing heat removal from all four lateral faces. The holder was water-cooled to 12 °C. The SA was inserted between the laser element and the OC. All optical elements were positioned as close as possible to reduce the cavity round trip time. The total geometrical cavity length was  $\sim 7 \text{ mm}$ . The laser element was pumped through the PM with a CW Tm fiber laser (IPG Photonics) emitting up to 5.1 W at 1.91  $\mu\text{m}$  with a spectral linewidth of 0.7 nm. The Tm fiber laser provided a collimated unpolarized output beam, 4.5 mm in diameter, a full divergence angle of 0.58 mrad and  $M^2 = 1.05$ . The pump beam was focused into the sample by a 50 mm focal length lens. The mean radius of the pump beam in the sample was  $w_p = 150 \pm 10 \mu\text{m}$  (it was placed slightly out of focus to ensure better mode-matching). The total pump absorption under lasing conditions was  $\sim 33 \pm 2\%$ , as determined based on the small-signal pump-transmission measurements and rate-equation modelling accounting for ground-state bleaching, see details in [24].

Commercial SSAs (BATOP, model SA-2000-1-25.4g) were used for PQS, see inset in Fig. 1(c). The transmission-type SSAs were AR/AR-coated around 2  $\mu\text{m}$ . Each SSA was mounted on a passively-cooled Cu-holder. The specified characteristics of the SSAs were as follows: small-signal absorption at 2000 nm  $\alpha'_0 = 1\%$ , fraction of the saturable losses  $\alpha'_s/\alpha'_0 = 0.5$ , saturation fluence  $F_{\text{sat}} = 300 \mu\text{J}/\text{cm}^2$  and recovery time  $\tau_{\text{SA}} = 7, 13$  or 21 ps for different SSAs. At the emission wavelength of the Ho:YAG ceramic, according to the absorption spectrum, Fig. 1(c), the actual  $\alpha'_s = 0.24\%$ . The radius of the laser mode in the laser element and SA was  $\sim 145 \pm 5 \mu\text{m}$ , calculated with the ABCD method using a value for the sensitivity factor of the thermal lens of  $2.2 \text{ m}^{-1}/\text{W}$  [24]. The absorption of the SSAs at the pump wavelength (for the residual pump) in the bleached state was  $\sim 0.24\%$ .

A fast ( $\sim 30 \text{ ps}$ ) InGaAs PIN photodetector and a 1 GHz digital oscilloscope were used for detection of the Q-switched pulses.

## 3. Results and discussion

At first, we studied the CW performance of the Ho:YAG ceramic laser (when removing the SA from the laser cavity and moving the OC closer to the laser element). It generated a maximum output power of 1180 mW at 2090.4 nm with a slope efficiency  $\eta = 88\%$  with respect to the absorbed pump power,  $P_{\text{abs}}$ , Fig. 2. The laser threshold was at  $P_{\text{abs}} = 0.35 \text{ W}$  and the optical-to-optical efficiency with respect to the incident power was 23%.

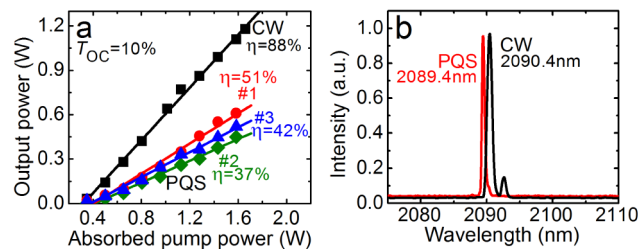


Fig. 2. CW and SSA passively Q-switched Ho:YAG ceramic laser: (a) input-output dependences,  $\eta$  - slope efficiency,  $\tau_{\text{SA}}$  - specified recovery time of the SSAs: #1 (7 ps), #2 (13

ps) or #3 (21 ps); (b) typical laser emission spectra,  $P_{\text{abs}} = 1.59$  W, the spectrum in the PQS regime corresponds to the SSA with  $\tau_{\text{SA}} = 7$  ps.

Inserting the SSAs into the laser cavity, stable PQS was achieved. For the SA with a specified  $\tau_{\text{SA}} = 7$  ps, the maximum average output power reached 610 mW at 2089.4 nm corresponding to  $\eta = 51\%$ . The conversion efficiency with respect to the CW operation mode  $\eta_{\text{conv}}$  amounted to 52%. The laser threshold was at  $P_{\text{abs}} = 0.40$  W and the optical-to-optical efficiency with respect to the incident power  $\eta_{\text{opt}}$  amounted to 13%. Using the SA with  $\tau_{\text{SA}} = 13$  ps and 21 ps, the laser performance was slightly inferior, Fig. 2(a), namely 450 mW with  $\eta = 37\%$  and 520 mW with  $\eta = 42\%$ , respectively. The input-output dependences for the Ho:YAG ceramic laser are clearly linear indicating no detrimental thermal effects. The measured laser emission spectra, Fig. 2(b), are in agreement with the gain spectra, Fig. 1(b). The laser output was unpolarized for both, the CW and PQS regimes. The output mode of the laser corresponded to  $\text{TEM}_{00}$ .

The use of SSAs with different  $\tau_{\text{SA}}$  resulted in similar pulse characteristics, Fig. 3, with clear dependence on the absorbed power. This effect is typical for “fast” SAs and related to the different bleaching of the SA with an increase of  $P_{\text{abs}}$ . In particular for the SA with  $\tau_{\text{SA}} = 13$  ps, the pulse duration  $\Delta\tau$  (determined as FWHM) decreased from 250 to 89 ns with  $P_{\text{abs}}$  and the pulse repetition frequency (PRF) increased almost linearly from 7 to 141 kHz. The pulse energy  $E_{\text{out}}$  at the maximum pump power was  $\sim 3$   $\mu\text{J}$ . Consequently, the maximum peak power,  $P_{\text{peak}} = E_{\text{out}}/\Delta\tau$ , reached 36 W.

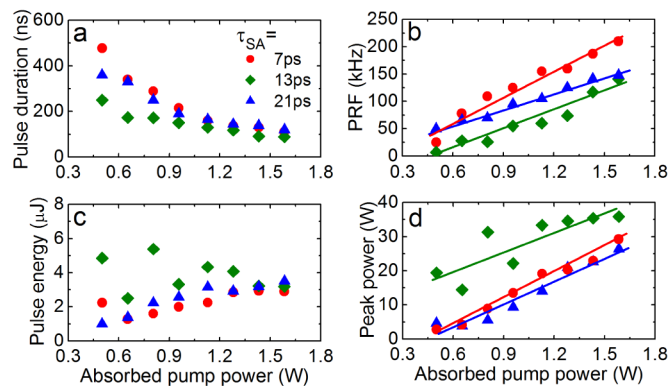


Fig. 3. SSA passively Q-switched Ho:YAG ceramic laser: pulse duration  $\Delta\tau$  (FWHM) (a), pulse repetition frequency (PRF) (b), pulse energy  $E_{\text{out}} = P_{\text{out}}/\text{PRF}$  (c) and peak power  $P_{\text{peak}} = E_{\text{out}}/\Delta\tau$  (d),  $\tau_{\text{SA}}$  – recovery time of the SSAs.

The oscilloscope traces of single Q-switched pulses obtained using the SSA with a specified  $\tau_{\text{SA}} = 13$  ps at various  $P_{\text{abs}}$  and the corresponding pulse train for the maximum  $P_{\text{abs}} = 1.59$  W are shown in Fig. 4. The intensity instabilities in the pulse train were  $<15\%$  and the pulse-to-pulse timing jitter was  $\sim 10\%$ . These instabilities are primarily attributed to the heating of the SSA due to absorption of the residual pump power.

No damage of the SSAs was observed during operation (the intracavity fluence on the SA reached  $0.2$   $\text{J}/\text{cm}^2$  and the corresponding intracavity intensity  $\sim 2.1$   $\text{MW}/\text{cm}^2$ ).

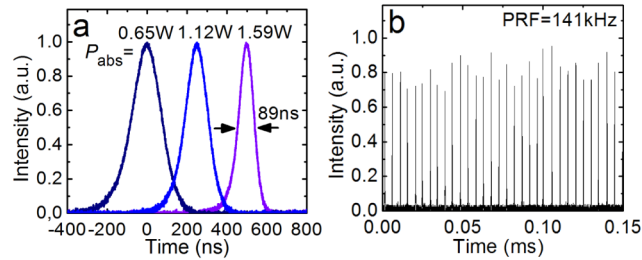


Fig. 4. Passively Q-switched Ho:YAG ceramic laser using the SSA with  $\tau_{SA} = 13$  ps: oscilloscope traces of the single pulses at various  $P_{abs}$  (a) and the corresponding pulse train for  $P_{abs} = 1.59$  W (b).

In Table 1, we compared the output characteristics of the passively Q-switched Ho:YAG ceramic lasers reported so far. The SSAs provide pulse characteristics similar to the “fast” SAs based on carbon nanostructures (graphene and SWCNTs) [24,25] with the same saturable absorption (0.2-0.4%) and to the semiconductor (PbS) quantum dots (QDs) in glass as the one described in [26] whilst the technology of the latter SAs is still far from being mature. Further shortening of the pulse duration when using SSAs for PQS of Ho lasers is possible by increasing their modulation depth which may lead to the generation of pulses with  $\Delta\tau$  of few ns and  $E_{out}$  of few tens of  $\mu\text{J}$  reaching kW peak powers. Further power scaling of such Ho lasers (which was limited in the present work by the available pump power and the low Ho doping) may potentially lead to PRFs in the MHz-range. The reduction of the Q-switching instabilities can be provided by eliminating the residual pump power, e.g. by increasing the Ho doping or applying dichroic coatings on the output face of the laser element.

Table 1. Comparison of Output Characteristics of the Ho:YAG Ceramic Lasers Passively Q-switched by “Fast” SAs Reported so Far

SA material	$\alpha'_s$ , %	$P_{out}$ , mW	$\eta$ , %	$E_{out}$ , $\mu\text{J}$	$\Delta\tau$ , ns	PRF, kHz	$P_{peak}$ , W	Ref.
SSA	0.24	610	51	2.9	110	210	26	This work
SSA	0.24	450	37	3.2	89	141	36	This work
SWCNTs	0.35	810	68	4.9	85	165	58	[24]
graphene	0.32	640	55	3.6	170	180	21	[24]
graphene	-	264	16.5	9.3	9000	28	1	[25]
PbS QDs [26]	<1.5	479	38	1.5	95	329	15	unpublished

#### 4. Conclusion

We report on the first holmium micro-laser PQS by semiconductor saturable absorbers (SSA). We have employed a Ho:YAG transparent ceramic in-band-pumped by a Tm fiber laser at 1.91  $\mu\text{m}$ , and a commercial transmission-type SSA designed for the 2  $\mu\text{m}$  spectral range. This laser generated pulses as short as  $\sim 100$  ns at repetition rates of 140-210 kHz with maximum output powers of 610 mW at 2089 nm corresponding to a maximum slope efficiency of 51%. Further pulse shortening and scaling of the pulse energy seem to be feasible with the increase of the modulation depth of the SSA at 2.1  $\mu\text{m}$ . Among others, SSA passively Q-switched Ho microchip lasers are attractive for seeding of high-pulse-energy Ho-doped amplifiers.

#### Funding

National Natural Science Foundation of China (61405171); Science and Technology Program of the Shandong Higher Education Institutions of China (J13LJ05); European Union’s Horizon 2020 research and innovation programme under grant agreement No 654148 Laserlab-Europe and under the Marie Skłodowska-Curie grant agreement No 657630.

#### Acknowledgments

P.L. acknowledges financial support from the Government of the Russian Federation (Grant 074-U01) through ITMO Post-Doctoral Fellowship scheme.